

# Chapter 1

## Introduction and Background

### High-power broad-area lasers

High-power broad-area (BA) lasers are edge-emitting semiconductor lasers with a lateral emission aperture of some tens to hundreds of micrometers which is wide compared to the emitting near infrared wavelength, making them the most efficient tool for conversion of electrical into optical energy. Due to their very high output power, high efficiency, small size and low cost in mass production there is a strong industry demand. Although they are mainly used as pump sources, their fields of application have diversified and they can be for example also employed for direct material processing or light detection and ranging (LiDAR) systems needed for autonomous driving.

For optical gain to arise in semiconductor lasers, population inversion is obtained by electrical pumping. To restrict the carrier flow and to obtain a large carrier density in the active region heterostructures with different band gap materials grown by metalorganic vapour-phase or molecular-beam epitaxy on a crystalline substrate are utilized. The broad-area lasers investigated in this thesis consist of n-doped  $\text{Al}_x\text{Ga}_{1-x}\text{As}$  confinement and cladding layers with appropriate Al mol fractions  $x$ , single InGaAs quantum-well (QW) active regions, p-doped confinement and cladding layers and a highly p-doped GaAs contact layer grown on a GaAs substrate, Fig. 1.1. The epitaxial structure is metalized with a gold contact and soldered p-side down on a CuW submount, Fig. 1.1(d). In high-power lasers large optical cavities are employed with a comparatively weak vertical waveguide to reduce facet load so that high output powers can be achieved even under continuous wave (CW) operation.

BA lasers reach extremely high output powers, but exhibit a complex non-stationary spatio-temporal and highly non-linear behavior as a result of the interaction of optical, electrical and thermal phenomena. Due to the interplay of spatial depletion of carriers by stimulated emission and the insufficiently fast transport of injected carriers into the depleted regions spatial hole burning occurs. On the one hand, the resulting increase of the real part of the refractive index in those regions creates a local waveguide and leads to self-focusing, which is sometimes referred to as “filamentation” [1, 2]. On the other hand, due to high stimulated recombination and reduced amplification, the carrier density and thus the optical gain is decreased in the created waveguide core, which leads to self-defocusing. The result is a highly dynamic optical field, that can be well described in the mode picture: Single mode emission becomes unstable just above threshold because, due to lateral spatial hole burning, any mode saturates the optical gain in those parts of the active layer where the mode intensity is high. The

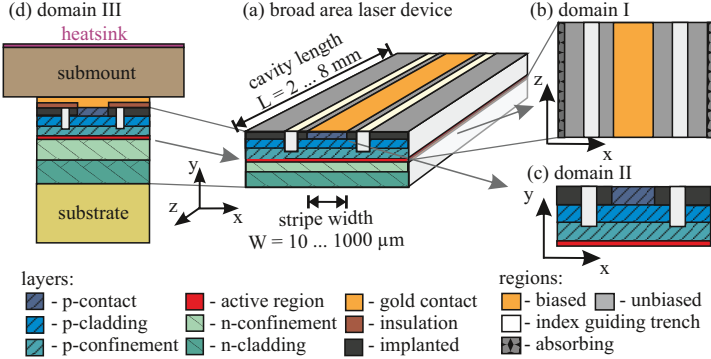


Figure 1.1: (a) Schematic representation of a BA laser and simulation domain of the (b) time-dependent traveling-wave and lateral carrier-diffusion equation, (c) inhomogeneous current-spreading model, and (d) heat transport equation. For lateral optical and current confinement index-guiding trenches can be etched. The electrical conductivity of the p-contact layer next to the injection stripe (opening of the insulation layer) is often reduced by ion implantation.

gain in other parts rises with current, bringing more modes to threshold which can be additionally supported by a built-in or thermally induced waveguide. In Zeghuzi et al., *IEEE J. Quantum Electron.*, 55(2):2000207, 2019 [3] the mode picture is supported by a theoretical analysis of the emitted laser field. The findings of [3] are discussed in more detail in Chapter 6.

A consequence of the highly dynamic field are fluctuating heat sources and a resulting non-stationary temperature profile. The time-dependent approach to thermal waveguiding and the resulting substantial refractive index changes and their significant impact on the optical field are presented in Zeghuzi et al., *IEEE J. Sel. Top. Quantum Electron.*, 25(6):1502310, 2019 [4] and discussed in more detail in Chapter 6.4.

Due to the broad emission aperture and the excitation of several lateral modes with higher near-field widths and far-field angles, BA lasers suffer from a bad lateral beam quality. It exceeds the diffraction limit already slightly above threshold, which limits the minimum achievable spot size of the emitted light. A measure of the lateral beam quality is the lateral beam parameter product  $\text{BPP}_{\text{lat}}$  or the beam quality factor  $M_{\text{lat}}^2$  which relates the beam quality to the beam quality of a Gaussian beam (for which  $\text{BPP}_{\text{lat}} = \lambda_0/\pi$ ),

$$\text{BPP}_{\text{lat}} = \frac{w_{0,\text{lat}}}{2} \cdot \frac{\Theta_{0,\text{lat}}}{2} = M_{\text{lat}}^2 \cdot \lambda_0/\pi \quad (1.1)$$

with the lateral near-field width  $w_{0,\text{lat}}$  and far-field angle  $\Theta_{0,\text{lat}}$  (see Fig. 1.2), and lasing wavelength  $\lambda_0$ . Thus, the BA laser community is facing the optimization problem of achieving high output powers  $P_{\text{out}}$  and a good beam quality  $\text{BPP}_{\text{lat}}$  at the same time, which are combined in the target figure of merit brightness

$$B_{\text{lat}} = P_{\text{out}}/\text{BPP}_{\text{lat}}, \quad (1.2)$$

that needs to be maximized.

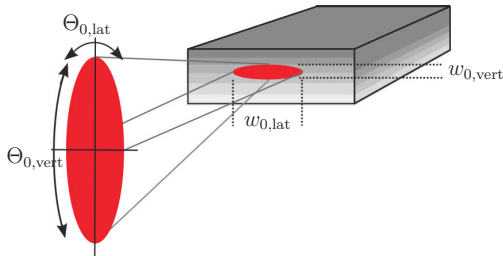


Figure 1.2: Sketch of a BA laser with emission characteristics.  $w_{0,\text{lat}}$  and  $w_{0,\text{vert}}$  denote the lateral and vertical near-field width and  $\Theta_{0,\text{lat}}$  and  $\Theta_{0,\text{vert}}$  the lateral and vertical far-field angle. Due to their broad emission stripe BA lasers suffer from a bad lateral beam quality.

With increasing current the slope of the power-current characteristics decreases due to power saturation. Under CW operation power saturation is mainly attributed to device heating as loss mechanism such as recombination, free carrier absorption and leakage currents are enhanced [5], whereas under pulsed operation, when nanosecond-current pulses with low repetition rates are applied, thermally induced power rollover is believed to be negligible. In this case non-thermal causes for power saturation are vertical carrier leakage and enhanced free-carrier absorption in the waveguide [6], longitudinal [7] and lateral [8, 9] spatial hole burning, two-photon absorption [10, 11], and mechanisms leading to gain compression [12][13], such as spectral hole burning and carrier heating as a result of finite intra-band relaxation times [14]. An analysis of the different non-thermal power-saturation effects has been published in Zeghuzi et al., *Opt. Quantum Electron.*, 50:88(1–12), 2018 [15] and is discussed in Chapter 5.

A very prominent effect that decreases the brightness is the broadening of the lateral far field with rising current (“far-field blooming“). Under CW operation it mostly results from the formation of a thermally induced waveguide, i.e. a substantial increase of the refractive index in the hot center below the contact stripe, commonly referred to as “thermal lensing“. This effect is well studied, both experimentally [16, 17] and theoretically [18, 19, 20], for CW operation assuming a stationary temperature distribution. Under pulsed operation it is usually neglected because thermal build-up times of up to milliseconds are much longer than the pulse lengths. However, the heat is generated near the active layer in the same region where the guided wave is localized. This region is small and its thermal build-up time is much shorter than that of the whole device. Accordingly, under pulsed operation short-time local heating is expected to influence the optical pulse formation although time-averaged heating is negligible. Results supporting this claim, have been published in [4] and are treated in Section 6.4.1.

Also non-thermal effects play a role in the broadening of the far field [21]. Non-thermal far-field blooming is a result of current spreading [21], lateral carrier diffusion and accumulation [22], and longitudinal and lateral spatial hole burning. Current spreading and lateral carrier diffusion and accumulation not only lead to an increased optical gain at the device edges but also modify the profile of the refractive index. Ultimately in both cases a larger number of higher-order lateral modes are excited.

## Semiconductor laser simulation models

The self-consistent simulation of the optical laser field, carrier transport and temperature is necessary to understand the spatio-temporal phenomena in BA lasers and to apply this knowledge in order to reduce costs for device optimization.

Due to the transverse instabilities present in BA lasers and the resulting non-stationary spatio-temporal behavior a time-dependent simulation model should be employed. Such a model needs to be sufficiently precise, whereas at the same time a good numerical performance is necessary to simulate real devices. Besides the highly dynamic and non-linear behavior, a main challenge for constructing such a model are the different time and length scales involved in the lasing process. The optical field, carrier density and temperature vary on time-scales of picoseconds, nanoseconds and microseconds, respectively, and the spatial scales of QW active region, epitaxial layers and lateral waveguide, as well as the length of the cavity range from nanometers, over micrometers to millimeters. Therefore, until now no simulation tool exists that covers all spatio-temporal scales and physical phenomena important for the description of BA lasers.

From the preceding observations it should be clear, that not all processes can be simulated on the same spatial and temporal grid and that approximations have to be made to simulate real devices within a reasonable time frame.

Generally the vertical epitaxial structure is designed to guide only a single mode. Its vertical profile remains mostly unchanged during the lasing process, so that the vertical dimension can be represented by a set of effective model parameters. Due to the nearly planar geometry of edge emitting lasers and their narrow-banded optical spectrum, in this thesis the optical field is represented by its transverse-electric  $x$ -component in the semiclassical framework of slowly-varying envelope, rotating-wave, scalar and paraxial approximations. The spatio-temporal evolution of the forward- and backward-traveling amplitudes is described by traveling-wave equations solved in the longitudinal-lateral  $(x, z)$ -plane displayed in Fig. 1.1(b) [23, 24].

The traveling-wave equations have to be coupled to the carrier reservoir via stimulated recombination and the optical field in turn is influenced by carrier density induced refractive index changes. For the description of the excess carriers in the active layer a lateral diffusion equation is solved. The injection current density entering this diffusion equation is gained self-consistently by solving the Laplace equation [18, 25] for the quasi-Fermi potential of the holes in the p-doped region sketched in Fig. 1.1(c). This model properly describes spatial hole burning, because the self-distribution of the current density is considered, as well as lateral current spreading. It is published in Zeghuzi et al., *Proc. SPIE*, 10526:105261H, 2018 [26] and discussed in Chapter 3 in more detail.

To self-consistently describe heating effects, the heat sources entering the heat-flow equation have to be calculated from the field intensity, carrier density and injection current density distributions. The resulting temperature influences the optical field via refractive index changes and temperature-dependent model parameters. However, the non-stationary heat-flow equation can't be solved on the same time and length scales as the electro-optical models. Thus in this thesis the rate of heat generation is decomposed into a time-constant mean contribution and a time-dependent fluctuating deviation from this mean value. For the treatment of pulsed operation inherent traits of heat generation and conduction can be exploited so that the temperature-induced

refractive index can be self-consistently derived from the heat sources for short pulse lengths. For CW operation the electro-optical models are iteratively coupled to the heat transport equations solved in the domain represented in Fig. 1.1(d). The heat model is published in [4] and discussed in more detail in Chapter 4.

The resulting time-dependent quasi-three-dimensional opto-electronic and thermal model describes well essential qualitative characteristics of real devices such as the multi-peaked, dynamic near-field structure, power-current characteristics, the time-averaged multi-peaked and not diffraction-limited near- and far-field intensities, as well as laser-output spectra.

Some laser simulation tools solve the full drift-diffusion equations to treat the current flow in the device and its interaction with the non-equilibrium carrier densities [21, 19]. These models are based on a stationary approximation and use for the description of the optical field either an expansion into linear waveguide modes [21] or a beam propagation method [19]. However, due to their inherently non-stationary and highly non-linear behavior the applicability of both methods to BA lasers is questionable. Indeed, these models do not converge at high optical output powers [27], so that spatio-temporal effects can be studied only slightly above threshold.

Due to computer restrictions, until now simulation tools based on the bidirectional traveling-wave model for the optical field [28, 29, 30] do not solve the time-dependent drift-diffusion equations, but only a lateral diffusion equation for the excess carriers in the active layer with a spatially constant injection current density below the contact stripe as source term. Such a constant-injection-current-density model, which is even used by stationary simulation tools [31, 32] oversimplifies the current flow and carrier transport in the device, because current spreading and current self-distribution are not included [33].

Theoretically, a time-dependent temperature has been considered in early models as presented in e.g. [34, 35], where they concentrated on a sophisticated microscopic description of the processes in the active layer. However, besides requiring enormous computational resources even for nanosecond transients, outer parts of devices are disregarded although a considerable portion of the heat is generated here. Heat flow was replaced by a simple local relaxation of temperature towards an ambient temperature. These features limit an application in device design.

The model proposed in this thesis is based on an existing model for the time-dependent traveling-wave equation [23]. Together with corresponding equations for the macroscopic polarization density to describe dispersion and a lateral diffusion equation for the excess carriers in the active region with a constant injection current density, this model has already been successfully applied to the simulation of a large variety of high-power laser structures [36, 37, 38, 39, 40, 41]. The improvement of the model [23] is a central part of this thesis, whereas the numerical modeling and implementation was performed by M. Radziunas and J. Fuhrmann at the Weierstrass Institute for Applied Analysis and Stochastics (WIAS). Details on the numerical modeling and used schemes can be found in [23, 42, 43, 44] and in Appendix D.

## Objectives and structure of this work

The subject of this work is the analysis of spatio-temporal phenomena in BA lasers and the mitigation of effects that limit their lateral brightness. To this end a simulation

model that is sufficiently precise and yet numerical applicable is derived and applied for lateral brightness optimization for pulsed and CW operation.

The following three chapters describe the time-dependent quasi-three-dimensional opto-electronic and thermal model. In Chapter 2 the parabolic paraxial wave-equation is presented that bases on the slowly-varying amplitude, rotating-wave and effective-index approximations, taking into account gain dispersion, spontaneous emission, periodic corrugations of the refractive index (i.e. Bragg gratings) and a third-order nonlinear susceptibility. In Chapter 3 the basic drift-diffusion equations will be presented. They will be reduced to an effective diffusion equation in the active region with a carrier density dependent diffusion coefficient. An advanced model for the injection current density is derived that adequately describes current self-distribution and spreading in the p-doped layers. In Chapter 4 the energy-transport model which bases on [45, 46] is summarized, paying particular attention to a consistent formulation with the model for the optical field in Chapter 2. A temperature model is presented that can self-consistently derive short-time local heating near the active region as well as the formation of a stationary temperature profil by an iterative coupling of the electro-optical models to the heat transport equations.

Chapter 5 deals with non-thermal power saturation that limits the achievable output power and as a result the brightness at high injection currents under pulsed operation. Power saturation resulting from spatial hole burning, current spreading and two-photon absorption and the impact of spatio-temporal fluctuations on the output power are discussed whereas additional effects can be included in the theoretical model by a gain compression term. The simulation results are compared to experiments.

In Chapter 6 phenomena that influence the lateral field distribution in BA lasers are examined. In the first part two mechanisms that are generally referred to when it comes to the understanding of the multi-peaked lateral field profile are discussed. On the one hand the Bespalov Talanov modulation instability [47] is investigated that describes the spontaneous break-up of the optical field into small filaments. On the other hand the decomposition of the field retrieved from the traveling wave equations into lateral waveguide modes is described. This procedure will then be used in the following sections for the investigation of the lasing process with regards to the mode picture. In the second part of Chapter 6 the non-thermal broadening of the far field with current and its dependence on series resistivity, sheet resistance, mobility, as well as carrier induced refractive index changes is investigated. These effects are discussed in the mode picture and possibilities for beam quality improvement are derived. In the last part of Chapter 6 the influence of slow and fast contributions to the time-dependent temperature on the lateral near- and far-field distributions are investigated. On the one hand, the effect of a thermally induced waveguide under short pulse operation with extremely high injection currents is exemplary investigated for laser operation with 10 ns long pulses. On the other hand the time-dependent approach to CW operation is discussed. In particular the strong spatio-temporal sub-nanosecond fluctuations of the heat sources on wave propagation are examined. Furthermore the front facet near-field narrowing as a result of the time-averaged longitudinally varying temperature profile is derived self-consistently. To counteract it, index-guiding trenches filled with an insulator can be etched next to the injection stripe. The simulation results are compared to experiments.

In Chapter 7 methods for the improvement of the lateral brightness are discussed. In the first part of Chapter 7 the brightness improvement by varying the built-in index step of index-guiding trenches, their width and distance to the injection stripe will be

discussed. A further current-path tailoring by deep implantation of the laser next to the injection stripe is investigated as well. The simulation results are compared to experiments. In the second part of Chapter 7 a lateral and longitudinal structuring of the contact region is investigated. Laser arrays show a narrow single lobe around  $0^\circ$  far-field angle when the fields in each stripe element are co-phasal. As this is only achieved at currents near threshold, additional mode-selection mechanisms are discussed, such as a Talbot-type spatial filter where free running sections with lengths corresponding to half the Talbot length are alternately included. An additional longitudinal structuring with periods corresponding to the Talbot length and additional phase tailoring for the suppression of the out-of-phase mode are investigated. The simulation results are compared to experiments.



# Chapter 2

## Optical field model

To model laser operation far above threshold the electromagnetic field can be treated semiclassically by the Maxwell equations with a spontaneous current-density sources term [48, 49]. The full vectorial wave equation can be significantly simplified using certain properties of the emitted laser light: The investigated edge emitting devices are longitudinally more extended than laterally and the emitted laser light has a dominant propagation in  $z$ -direction. The growth direction ( $y$ -direction) defines a nearly planar geometry, so that the optical field is expressed by its transverse-electric  $x$ -component. As the transverse refractive index changes are small and the laser emits in a small frequency band around a central frequency further approximations can be made.

Accordingly a parabolic paraxial wave-equation for the slowly-varying forward- and backward-traveling field envelopes are gained as described in Section 2.1. The traveling-wave equations are coupled to dynamic equations for the macroscopic polarization density and carrier density, so that this set of equations is formally similar to the system of Maxwell-Bloch equations for a two level atom [28]. In Section 2.2 a balance equation for the radiative energy density and the associated energy flux given by the Poynting vector is derived. Supposing a well-designed vertical waveguide, the normalized fundamental vertical mode  $\phi(y)$  remains unchanged during laser operation. Accordingly the vertical direction can be represented by effective model parameters. This approximation termed “effective index method” is explicitly executed in Section 2.3 to clarify the derivation of model parameters. Together with the model equations presented in Chapter 3 and 4 for the carrier density and temperature this system of equations describes well essential qualitative characteristics of real devices. The retrieval of the corresponding characteristics that can be used to compare to experimental data is described in more detail in Section 2.4.

### 2.1 The traveling-wave equations

The governing optical equations can be derived semiclassically from Maxwells equations using a spontaneous current-density source term. A detailed derivation can be found in [49]. Here, the important approximations and underlying properties of the emitted laser light are shortly recapitulated.

As a result of the nearly planar geometry of edge emitting semiconductor lasers defined by the epitaxial layer structure the electromagnetic field is either mainly transverse electric (TE) or transverse magnetic (TM) polarized. In this work the optical field is represented by its transverse-electric  $x$ -component. Furthermore the electric

field is separated into forward- and backward-traveling wave amplitudes  $E^\pm(\vec{r}, t)$  and by choosing an appropriate reference wave vector  $\bar{n}k_0$ , where  $\bar{n}$  is the real valued reference index and  $k_0$  the free-space wavevector, and center frequency  $\omega_0$ , the transverse-electric optical field is represented by

$$\vec{E}(\vec{r}, t) = \vec{e}_x \frac{1}{2} E(\vec{r}, t) e^{i\omega_0 t} + \text{c.c.} \quad (2.1)$$

$$\text{with } E(\vec{r}, t) = E^+(\vec{r}, t) e^{-i\bar{n}k_0 z} + E^-(\vec{r}, t) e^{i\bar{n}k_0 z} \quad (2.2)$$

and  $k_0 = 2\pi/\lambda_0$  with the center wavelength  $\lambda_0$ .

Several important properties of the emitted laser light can be used to significantly simplify the wave equation. Firstly, the wave propagation within a laser resonator has a dominant propagation direction (here  $z$ -direction). Furthermore lasers generally emit within a small frequency range around a center frequency  $\omega_0$  corresponding to the optical transitions in the active material. Thus, it can be assumed that the envelopes of the forward- or backward-traveling waves  $E^\pm(\vec{r}, t)$  vary slowly in time and space compared to the optical wavelength or spatial period defined in Eqs. (2.1) and (2.2) by the reference wave vector  $\bar{n}k_0$  and center frequency  $\omega_0$ .

This slowly-varying envelope approximation implies, that the second  $z$ -derivative of the electric field  $|\partial_z^2 E^\pm|$  is small against  $|2\bar{n}k_0 \partial_z E^\pm|$  (paraxial approximation) and likewise that the second time derivative  $|\partial_t^2 E^\pm|$  is small against  $|2\omega_0 \partial_t E^\pm|$  and that both can be neglected in the final equation. Based on the same assumption, terms that rapidly oscillate in time  $e^{i2\omega_0 t}$  (rotating wave approximation) and space  $e^{\pm i2\bar{n}k_0 z}$  can be neglected.

Furthermore, due to the small transverse refractive index change only the scalar wave equation has to be solved. Taking into account these approximation the slowly-varying envelope amplitudes of the forward- and backward-traveling waves obey the traveling-wave equation [49]

$$\begin{aligned} \frac{1}{v_g} \partial_t E^\pm(\vec{r}, t) \pm \partial_z E^\pm(\vec{r}, t) &= -\frac{i}{2\bar{n}k_0} (\partial_x^2 + \partial_y^2) E^\pm(\vec{r}, t) \\ &- \frac{ik_0}{2\bar{n}} \Delta n^2(\vec{r}, t) E^\pm(\vec{r}, t) - \frac{ik_0 n_r \varepsilon_0 c}{2} \Delta n_2(\vec{r}, t) [ |E^\pm(r, t)|^2 + 2|E^\mp(r, t)|^2 ] E^\pm(\vec{r}, t) \\ &- ik_0 \frac{\eta^\pm(r, \omega_0)}{2\bar{n}} E^\mp(r, t) - \frac{n_r(\vec{r}, t) G_r(\vec{r}, t)}{2\bar{n}} [ E^\pm(\vec{r}, t) - \mathcal{P}^\pm(\vec{r}, t) ] + F_{\text{sp}}^\pm(\vec{r}, t). \end{aligned} \quad (2.3)$$

Here  $v_g = c/n_g$  is the group velocity with the speed of light  $c$  and group index  $n_g = \bar{n} + \omega_0 \partial_\omega \bar{n}(\omega)|_{\omega=\omega_0}$  and  $\varepsilon_0$  the vacuum permittivity.

The first term on the right hand side of Eq. (2.3) accounts for transverse refraction of the optical field.  $\Delta n^2(\vec{r}, t)$  describes the deviation of the complex refractive index  $n^2 = 1 + \chi$  to the real valued reference index  $\bar{n}^2 = 1 + \bar{\chi}$ , where  $\chi$  and  $\bar{\chi}$  are the complex and real valued reference susceptibilities, respectively,

$$\Delta n^2(\vec{r}, t) \equiv n^2(\vec{r}, t, \omega_0) - \bar{n}^2 = \Delta n_r^2(\vec{r}, t) + i \frac{n_r(\vec{r}, t) [g(\vec{r}, t, \omega_0) - \alpha(\vec{r}, t)]}{k_0}.$$

Here  $\Delta n_r^2$  is the real part of  $\Delta n^2$ ,  $n_r$  the real part of  $n$  and  $g$  and  $\alpha$  the coefficients of optical gain and absorption due to transitions between the conduction and valence bands, respectively. The coefficient of the optical gain  $g$  couples the traveling-wave equation for the optical field to the dynamic rate equation of the carrier reservoir (3.39)